ROTATIONAL TEMPERATURE MEASUREMENTS 300° K TO 1000° K WITH ELECTRON BEAM PROBE

By William W. Hunter, Jr.

NASA Langley Research Center
Langley Station, Hampton, Va.

Presented at the ISA Twenty-First Annual Conference and Exhibit

New York, New York
October 24-27, 1966

[redacted]

ROTATIONAL TEMPERATURE MEASUREMENTS 300° K TO 1000° K WITH ELECTRON BEAM PROBE

by William W. Hunter, Jr.
Physicist
NASA Langley Research Center
Langley Station, Hampton, Va.

ABSTRACT

Laboratory measurements of rotational temperatures were performed over a 300° K to 1000° K range in static low-density air with an electron beam probe. The accuracy of the measured rotational temperatures was found to be a function of gas number density and temperature. Inclusion of an experimentally determined correction for the gas number density effect enabled measurements to be made with an accuracy that varied approximately from 0 percent to -6 percent with increasing gas temperature.

INTRODUCTION

The investigations described in this paper were undertaken as part of a continuing instrument development program at NASA's Langley Research Center. This particular effort was directed towards the verification of a technique for measuring free-stream temperatures of low-density hypersonic wind tunnels using air or N_2.

The technique is to pass a beam of high-energy electrons (10 to 30 kV) through a low-density gas. The electrons have inelastic collisions with gas molecules which produce fluorescence. A spectral analysis of the fluorescence provides a means for determining molecular gas rotational temperature.

The initial investigator, E. P. Muntz,[1] experimentally verified his theoretical model for the electron beam probe technique for two temperatures, ≈300° K and 373° K. These experiments were conducted in a low-velocity (0.5 m/sec) flow of nitrogen gas and the data were obtained from the 0-0 band of the nitrogen first negative system. Since the original work, others,[2,3,4,5] have used the technique for diagnostic wind-tunnel measurements. Some have used the calculated tunnel parameters for comparison with the measured temperatures as a test of the theory for temperatures below 300° K.[4]

The purpose of the work reported here was to experimentally verify the theory for rotational temperature measurements over a 300° K to 1000° K range under controlled conditions in the laboratory. These tests were conducted in a static test gas, air, and the rotational temperature measurements were made from data obtained from the 0-0 band of nitrogen.

The procedure for this investigation was to pass high-energy electrons through the static test gas which was at a known temperature. The gas was contained in a test chamber which could be maintained at a desired temperature and pressure. With the test gas under controlled conditions, measurements of the rotational temperature were performed and compared with a reference temperature. This comparison provided the basis for determining the applicability of the theory over a range of temperatures.

The first portion of this paper outlines the theory. This is followed by a description of the experimental system, test procedure, the experimental data, and results.

THEORY

General

The test gas used in this investigation was air and the primary sources of visible and near ultraviolet radiation were the first negative and second positive systems of nitrogen. The excitation and emission path for the first negative system is illustrated by an energy level diagram in Figure 1. A high-energy electron, designated as a primary electron, is emitted by a source and has an inelastic collision with a ground state nitrogen molecule, $N_2X^1\Sigma_g^+$. The molecule is excited to the excited ionized state, $N_2^+B^2\Sigma_u^+$, from which it spontaneously radiates and drops into the ground ionized energy state, $N_2^+X^2\Sigma_g^+$. The intensity and spectral distribution of the spontaneous emitted radiation reflects the rotational characteristics of the molecules that were in the $N_2X^1\Sigma_g^+$ state.

Rotational temperature may be obtained from an application of the intensity of emission equation

$$I_{em}^{nm} = N_n h c \nu_{nm} A_{nm} \qquad (1)$$

Superior numbers refer to similarly numbered references at the end of this paper.

where $hc\nu_{nm}$ is the energy of the emitted radiation as a result of the transition between states n and m, ν_{nm} is the wave number of the emitted radiation, A_{nm} is the transition probability of emission, and N_n is the number density population of the initial level of transition. An inspection of equation (1) shows that all terms are constants or dependent only on the particular transition involved except N_n. Application of equation (1) requires the determination of the population and its distribution in the initial level, $N_2^+B^2\Sigma_u^+$.

Based on arguments presented in reference 1, it is assumed that $N_2^+B^2\Sigma_u^+$ is populated primarily by ionized and excited molecules from $N_2X^1\Sigma_g^+$. Population contributions from other possible origins are neglected. Therefore, the population of the rotational energy states of $N_2^+B^2\Sigma_u^+$ is determined by the excitation-transition process of $N_2X^1\Sigma_g^+$ molecules.

The excitation-transition process may be described through a Born-Oppenheimer approximation of the molecular wave function

$$\psi_{evJ\Lambda M} = \psi_e\left(\bar{r}_i,\bar{r}_N\right)\frac{1}{r_N}\,\psi_v\left(r_N\right)\psi_{J\Lambda M}(\theta,\chi,\phi) \qquad (2)$$

where ψ_e is the electronic wave function with the ith electronic coordinate $\bar{r}_i$ referenced to the molecular axis, ψ_v is the vibrational wave function with nuclei separation $\bar{r}_N$, and $\psi_{J\Lambda M}$ the rotational wave function which is a function of the Euler angles (θ,χ,ϕ). The Euler angles relate the molecular coordinate system to the coordinate system of the fixed point of observation. Also, it is assumed that the interaction of the primary electron with the orbital electrons can be described by a coulombic potential. Therefore, the following matrix element of this interaction may be used to describe the excitation:

$$\left(e_P,e_S,B^2\Sigma_u^+v'J'\Lambda'M'\left|\sum_i\frac{e^2}{r_{1i}}\right|e_P,X^1\Sigma_g^+v''J''\Lambda''M''\right) \qquad (3)$$

In the above expression, the initial and final wave functions of the primary electrons are represented by e_P'' and e_P', e_S' the secondary electron, $X^1\Sigma_g^+$ and $B^2\Sigma_u^+$ represent the initial and final electronic wave functions, v'' and v' the vibrational states, and $J''\Lambda''M''$ and $J'\Lambda'M'$ the rotational states. Of course, $\sum_i \frac{e^2}{r_{1i}}$ is the coulombic interaction term where the quantity r_{1i} is the distance between the high-energy primary electron and the ith orbital electron.

It should be noted that in the notation to be used, prime superscripts refer to $N_2^+B^2\Sigma_u^+$ states, double prime superscripts with a one (1) subscript refers to $N_2X^1\Sigma_g^+$ states, and double prime superscripts with a two (2) subscript refer to $N_2^+X^2\Sigma_g^+$ states.

Since the particular transition of interest results in the removal of one orbital electron and for simplicity $\sum_i \frac{1}{r_{1i}}$ will be replaced with $\frac{1}{r_{12}}$ where the removed electron is labeled with a subscript 2. The removed orbital electron is a $\sigma_u 2s$ electron[6] from $N_2X^1\Sigma_g^+$ to form $N_2^+B^2\Sigma_u^+$, therefore, the electronic state may be expressed as $X^1\Sigma_g^+ \equiv \left[B^2\Sigma_u^+\sigma_u 2s\right]$ Equation (3) is now rewritten as

$$\left(e_P,e_S,B^2\Sigma_u^+v'K'\Lambda'M'\left|\frac{e^2}{r_{12}}\right|e_P''\left[B^2\Sigma_u^+\sigma_u 2s\right]v''K''\Lambda''M''\right) \qquad (4)$$

Note that K has been used in place of J; this may be done from consideration of the applicable coupling scheme which is Hund's case (b)[6] and by suppressing the spin angular momentum.

In order to evaluate this matrix element for high-energy primary electrons, a plane wave approximation is made for the primary electron wave functions and the integration over the primary electron coordinates is performed. This integration gives[7]

$$\int e_P'\left(\bar{r}_1\right)\left(\frac{1}{r_{12}}\right)e_P''\left(\bar{r}_1\right)d\bar{r}_1 = \frac{4\pi}{q^2}\,e^{i\bar{q}\cdot\bar{r}_2} \qquad (5)$$

where $\bar{q}$ is the momentum transfer and $\bar{r}_2$ is the position vector of the interacting orbit electron. At this point a series expansion of $e^{i\bar{q}\cdot\bar{r}_2}$ is made

$$e^{i\bar{q}\cdot\bar{r}_2} = 1 + i\bar{q}\cdot\bar{r}_2 - \frac{1}{2}\left(\bar{q}\cdot\bar{r}_2\right)^2 + \ldots \qquad (6)$$

To a first-order approximation the first two terms of the above expansion are retained. But the contribution from the first term in equation (6) is zero because of the orthogonality of the initial and final states of the molecule. Therefore, equation (4) is given by

$$\frac{4\pi}{q^2}\,e^2\left(e_S,B^2\Sigma_u^+v'K'\Lambda'M'\left|i\bar{q}\cdot\bar{r}_2\right|\left[B^2\Sigma_u^+\sigma_u 2s\right]v''K''\Lambda''M''\right) \qquad (7)$$

In order to evaluate equation (7) further, the vector $\bar{r}_2$ is transformed to the coordinates of the molecular axis through the dyadic $\bar{\bar{D}}(\theta,\chi,\phi)$ which relates the molecular coordinate axis to the fixed coordinate system of the point of observation. Therefore, equation (7) is rewritten

$$\frac{i4\pi^2\bar{q}}{q^2} \cdot \left(K'\Lambda'M'\left|\bar{\bar{D}}(\theta,\chi,\phi)\right|K''\Lambda''M''\right)$$

$$\cdot \left(e_s, B^2\Sigma_u^+ v' \left|\left|\bar{r}_2'\right|\left[B^2\Sigma_u^+\sigma_u 2s\right]_{v''}\right.\right) \qquad (8)$$

The absolute value squared of the term $\frac{i4\pi e^2\bar{q}}{q^2}$ is contained in the excitation function, C_e, and will be suppressed in the following equations.

Evaluation of equation (8) shows that for the case $\Lambda'' = \Lambda' = 0$ only odd ΔK transitions are allowed. Most significant point is; not only $\Delta K = \pm 1$ transitions are permitted, as assumed in reference 1, but $\Delta K = \pm 3$, ± 5, and etc. are also permitted. Of course the cross sections for the $\Delta K = \pm 3$, ± 5, and etc. excitation-transitions will determine the contribution to the population of the excited state. This contribution is expected to be small.

The square of the second matrix element in equation (8) is defined as the band strength or the vibrational transition probability and is designed $P_{v'v''}$. This band strength $P_{v'v''}$ may be approximated by assuming a mean value of the internuclear separation. The second matrix element of equation (8) may then be written

$$P_{v'v''} = \left|\left(e_s, B^2\Sigma_u^+\left|\bar{r}_2'\right|\left[B^2\Sigma_u^+\sigma_u 2s\right]\right)\right|^2 \left|(v'|v'')\right|^2 \qquad (9)$$

The overlap integral of the vibrational wave functions squared $|(v'|v'')|^2$ is the well-known Franck-Condon factor, $q_{v'v''}$. Generally, equation (9) is then expressed as

$$P_{v'v''} = \left|R_{ij}^e\right|^2 q_{v'v''} \qquad (10)$$

In order to take into account the variation of internuclear separation, a method of $\bar{r}$ centroids[8] is used where $\bar{r}$ is the expectation value of the internuclear separation, r_N, as determined by the vibrational wave functions. Now, the band strength is given by

$$P_{v'v''} = \left|R_{ij}^e\left(\bar{r}_N\right)\right|^2 q_{v'v''} \qquad (11)$$

The rotational line strength is given by the first matrix element of equation (8) squared, summed over M'' and M'

$$\sum_{M'M''} \left|\left(K'\Lambda'M'\left|\bar{\bar{D}}\right|K''\Lambda''M''\right)\right|^2 \qquad (12)$$

This term is the well-known Hönl-London factor $S_{K''\Lambda''}^{K'\Lambda'}$ which is well tabulated.[6] For the transition of interest, the relative rotational line strength may be obtained through the ratio of the line strength to the sum of the line strengths, that is,

$$P_R^a = \frac{S_{K''}^{K'}}{\sum_{K'} S_{K''}^{K'}} \qquad (13)$$

This equation is the relative line strength for excitation-transition which is indicated by the superscript a. The relative line strength for emission is the same except the summation is over K'' and is designated P_R^e.

The preceding work of this section has been based on a plane wave approximation for the high-energy incident primary electron. It is necessary to consider low-energy secondary electrons since these may contribute significantly to the number of ionized nitrogen molecules. Several observations may be made without making a detailed analysis of the excitation-transition process. It should be noted that for electronic states of the homonuclear nitrogen molecule, $X^1\Sigma_g^+$ and $B^2\Sigma_u^+$ rotational levels have symmetric and antisymmetric states under nuclear exchange. The symmetry properties of $X^1\Sigma_g^+$ and $B^2\Sigma_u^+$ are the opposite with respect to even and odd rotational quantum numbers. And, only transitions between rotational energy levels with the same symmetry are allowed. Therefore, the same selection rules with respect to ΔK for high-energy electrons apply to low-energy electrons. The only difficulty would be if the first-order approximation is not sufficiently accurate such that $\Delta K = \pm 3$ or other transitions would contribute appreciably in order to describe secondary electron-induced transitions.

Rotational Temperature, T_R

The rotational number density, $N_{K'}$ of $N_2^+B^2\Sigma_u^+$, is a function of the excitation-transition process, depopulation rate, and number density, $N_{K_1''}$ of $N_2X^1\Sigma_g^+$. If it is assumed that rotational states of a v_1'' are in thermal equilibrium, then $N_{K_1''}$ is given by[6]

$$N_{K_1''} = \frac{N_{v_1''}}{Q_r}\left(2K_1'' + 1\right)e^{-E_{K_1''}/kT_R} \qquad (14)$$

where $Q_r = \sum_{K''} (2K'' + 1)e^{-E_{K_1''}/kT_R}$ is the rotational partition function, $E_{K_1''} = F\left(K_1''\right)hc$ the characteristic energy of a rotational state, $F\left(K_1''\right)$ the rotational term, and T_R the rotational temperature. Notice that a relation to a temperature has been established through the Boltzmann factor based on the explicit assumption that thermal equilibrium exists in the ground electronic state of the neutral species of N_2.

In order to interpret this temperature dependence in the resulting intensity of radiation, the selection rules for transitions between various rotational energy states are applied. As a first approximation the applicable selection rule for the excitation-transition process is

taken to be $\Delta K = \pm 1$. The $\Delta K = \pm 1$ selection rule predicts the formation of a P branch and R branch in the rotational fine structure of a vibrational band in excitation as well as emission. Shown in Figure 2 are the R and P branches of the 0-0 band of N_2^+.

With the formation of the P and R branches the steady-state population of $N_2^+ B^2\Sigma_u^+$ is given by*

$$N_{K'} = C_e' \sum_{v_1''} \left\{ \left[N''_{K''-1} P^a_{RR} + N'_{K''+1} P^a_{RP} \right] \cdot P_{v'v_1''} \right\} \quad (15)$$

where P^a_{RR} and P^a_{RP} are the relative rotational line strengths of absorption, previously described, for the P and R branches.

With the determination of $N_{K'}$, the intensity of emitted radiation may be calculated as a function of the rotational temperature, T_R. Before the calculation may be accomplished, it is necessary to set up an expression for the emission transition probability, $A_{v'K',v_2''K_2''}$

$$A_{v'K',v_2''K_2''} = X\nu^3 P_{v'v_2''} P^e_R \quad (16)$$

where X is a constant, ν is the wave number of the transition, and P^e_R is the relative rotational transition probability for emission.

The intensity of emission for a particular R-branch transition is given by

$$I_{K'K_2''} = XC_e'\nu^4 \sum_{v_1''} \left[\frac{\frac{N_o}{Q_r} e^{-E_{v_1''}/kT_v} P_{v'v_1''}(A)}{Q_r} \right] \left(\frac{K'}{2K'+1} \right) P_{v'v_2''} \quad (17)$$

where

$$(A) = K' e^{-E_{K'-1}/kT_R} + (K'+1) e^{-E_{K'+1}/kT_R} \quad (18)$$

This equation is simplified by noting that the product

$$XC_e' P_{v'v_2''} N_o / Q_v \quad (19)$$

is a constant, Z, for a particular $v' - v_2''$ transition. Also, the equation may be put in conventional form[6] by noting that $2K' = K' + K_2'' + 1$ for R-branch transitions. Therefore,

$$\frac{I_{K'K_2''}}{K' + K_2'' + 1} = \frac{Z\nu^4}{2(2K'+1)} \sum_{v_1''} \left[\frac{P_{v''v_1''} e^{-Ev_1''/kT_v}(A)}{Q_r} \right] \quad (20)$$

For the case of $T_v \lesssim 800^\circ$ K, 99 percent of the total population is in the $v_1'' = 0$ level. Equation (20) may now be written

$$\frac{I_{K''K_2''}/I_o}{K' + K_2'' + 1} = Z''\nu^4 [G] e^{-B_o K'(K'+1)hc/kT_R} \quad (21)$$

where B_o is the rotational constant related to the vibrational level and

$$Z' = \frac{ZP_{v_o'} e^{-E_o/kT_v}}{2Q_r I_o} \quad (22)$$

and

$$[G] = \frac{K' e^{2B_o K'hc/kT_R} + (K''+1) e^{-2B_o(K'+1)hc/kT_R}}{2K'+1} \quad (23)$$

Note that a reference intensity I_o has been included to permit the measurements of relative intensities. The term $[G]$ involves T_R and requires a solution of equation (21) through a process of iteration.

Analysis of equation (20) also reveals that only a small error $\approx \pm 1$ percent will be introduced by extending the application of equation (21) to temperature of 1000° K. This analysis was performed by calculating a B_{eff} to replace B_o in equation (20).

For ease of application, equation (21) is put in the following form:

$$\frac{B_o hc}{kT_R} K'(K'+1) + Z'' = -2.3 \log_{10} \left[\frac{I_{K'K_2''}/I_o}{(K' + K_2'' + 1)\left\{ [G](\nu/\nu_o)^4 \right\}} \right] \quad (24)$$

where ν_o is a reference wave number used to normalize ν. Following reference 1, ν_o value is chosen for $K' - K_2'' = 3\text{-}2$ transition. Also, Z" is just $\log_{10} Z'$, which is a constant.

EXPERIMENTAL SYSTEM

Test Gas Temperature and Pressure Control System

The test gas temperature and pressure control system, Figure 3, was designed to provide

*The following derivation is similar to that of reference 1 by E. P. Muntz.

flexibility in temperature and vacuum test conditions. Temperature and pressure operating ranges are approximately 300° K to 1100° K and 6.7 to 133.3×10^{-3} N/m^2 (1 torr ≈ 133.3 newton/meter^2).

The major component of the system is the test chamber which consists of three concentric cylinders. The outer cylinder is a stainless-steel water-cooled jacket and is fitted with vacuum-tight water-cooled top and bottom covers. Each cover is fitted with large flanges, attached to extensions, for mounting test hardware. Three 7.6-cm-diameter optical grade quartz windows are located in the outer cylinder wall. The next concentric cylinder consists of a helically wound nickel ribbon heating element and is attached to ceramic supporting rods. Electrical connections are made to copper electrodes which extend through the outer cylinder. The inner cylinder is a 20-cm-diameter 38-cm-long stainless-steel electrostatic shield and is grounded together with the outer cylinder to prevent charge buildup on the walls. Also, the inner cylinder provides a more uniform heating surface for the test gas than would be provided by the ribbon heating element. The inner cylinder is equipped with end covers which have openings for passage of the electron beam. A 3.8-cm by 1.3-cm slit opening is provided in the cylinder wall and is located in line with one of the viewing windows of the outer cylinder.

Rectified heater current is supplied from a 440 Vac 3-phase system. Temperature control is provided by coarse and fine rheostats. Temperature is regulated within ±1 percent of the preset value by an on-off automatic pyrometer. An operating temperature of 1100° K is obtained for a heating element voltage and current of 35 Vdc and 50 amperes.

A 35 psi water cooling system is provided as a heat sink for the outer chamber wall and covers, as well as cooling the diffusion pump. An interlock system prevents operation of the heating system and diffusion pump unless proper cooling flow is established.

A 5 CFM mechanical pump, 750 liter/sec diffusion pump, cold trap and necessary isolating valves comprise the vacuum pumping system. A variable leak valve, with air dryer, in combination with the mechanical pump was used to maintain the test chamber at the desired pressure. For all experiments the chamber pressure was measured with a McLeod gage.

Test Chamber Temperature Survey

A series of tests was conducted to establish the test chamber gas temperature. The first test was a survey of the inner cylinder wall to determine the uniformity of the heating surface. This survey was performed with 12 thermocouples attached to the inner cylinder wall and located to give reasonable coverage. The results indicated that a ±20° K variation existed at 1100° K. This variation decreased with decreasing temperature. The second test was made to determine the effects on the test gas at the point of observation by the inner cylinder ends. This was necessary because the ends are not in close proximity to the heating element and therefore cooler than the side walls. A thermocouple was located on the bottom end plate near the chamber center line. The temperature of this point was the lowest temperature of the plate.

These wall temperature measurements were used to calculate the gas temperature on the center line. The results of the calculations show that the effects of the inner cylinder ends would lower the gas temperature at the midpoint of the cylinder no more than 4° K at 1100° K.

The final test was an independent measurement of the test gas temperature at the point of observation. These measurements were made with a thermocouple whose leads were brought in along the chamber center line and the junction located at the point of observation. Two thermocouple sizes, 0.1-mm and 0.5-mm diameters, were used to determine if there were significant heat losses at the point of observation due to thermocouple conduction. The data shows that conduction losses were negligible. The results are indicated in Figure 4. These data show that the gas temperature at the point of observation is lower than the mean wall temperature. This difference decreases with temperature and converges to zero at an ambient value of temperature. This difference is attributed to heat sinks provided by the observation and pumping ports.

Electron Beam System

The electron beam system is illustrated in a block diagram, Figure 5, and details of the electron gun are shown in Figures 6 and 7. The electron gun is a conventional point cathode system which has a directly heated hairpin tungsten filament, independent negative grid bias for current control and cathode focusing. The beam upon passage into the drift tube is magnetically focused and deflected. The focused beam passes through a 1.0-mm-diameter hole in a $2\frac{1}{2}$-cm-long plug which is placed in the end of the drift tube. Because of the low gas conductance of this passage through the plug the test chamber may be operated at pressures approaching 133 N/m^2 while maintaining the gun within acceptable pressure range of 2.7×10^{-2} N/m^2 or less.

For the work reported here the beam system was operated at potentials between 25 and 30 Kv with currents of 1.0 to 1.5 ma. The beam potential and currents were held constant within ±1 percent of the selected valves for all tests.

Optical and Electronic Detector System

The major component of the optical and electronic detector system is the 0.5-meter Fastie-Ebert mount scanning spectrometer. This instrument has 16.0 Å/mm dispersion in the first order and a 0.2 Å resolution. A 13-stage venetian-blind photomultiplier tube which has a S-13 spectral response characteristic is mounted at the exit slit. The photomultiplier output is fed into an electrometer amplifier which drives a strip chart recorder. The overall response of the system is approximately 1 second. Based on the relatively slow response of the system, a 5 Å/min scanning speed was used.

ROTATIONAL TEMPERATURE MEASUREMENTS

300° K to 1000° K T_R Experiments

Rotational temperature measurements were made in air at approximately 100° K intervals from 300° K to 1000° K. This procedure was performed for three sets of experiments. Two sets of experiments were performed with a constant gas number density of $1 \times 10^{16}/cm^3$ and the other with a constant number density of $5 \times 10^{15}/cm^3$. The rotational temperature measurements were made from the 0-0 band first negative system of nitrogen. Typical spectral traces are shown in Figure 8.

The procedure for the rotational temperature measurement is to measure the peak value of a rotational line and enter this value into equation (24) for $I_{K'K''_2}$. It is necessary at this point to make an estimate of the rotational temperature by noting the rotational line at which maximum intensity is recorded. With the aid of this estimate, a value for $\left\{[G](\nu/\nu_o)^4\right\}$ is determined from table 1. This procedure is repeated for each rotational line. The next step is to plot each point, for strong lines, on a graph (e.g., Fig. 9), then by least squares fit determine the best straight line. From the slope of the curve a rotational temperature may be determined. If this value does not agree with the estimated value, the process is repeated with another temperature estimate and this process is repeated until the estimated and calculated temperatures fall within the smallest temperature division of the table of $\left\{[G](\nu/\nu_o)^4\right\}$ values. The entire procedure is repeated for the weak line system of the band. The final measured rotational temperature is determined from a weighted mean average of the values obtained from the strong and weak line systems.

Results of these tests are given in Figure 10 as a plot of the percent difference between weighted mean value of the rotational temperatures and the reference temperature versus the gas reference temperature. The gas reference temperature is the mean value wall temperature of the chamber corrected in accordance with Figure 4. There are two distinct groups of data, each corresponding to measurements made at different gas number densities. Two other points should be noted also. The first is the general trend of the data indicating a change in the percent difference between the measured value and reference temperatures with increasing gas temperature. The second is that the measured rotational temperature is high at ambient temperature and the difference increased with an increase in gas number density. This result indicated that the measured rotational temperature was dependent on gas number density.

T_R Gas Number Density Dependence

In several cases investigators[1,4] have pointed out that T_R measurements made in a static gas were higher than the reference temperature and appeared to be a function of gas number density. Because of these observations and results given above, tests were conducted to determine T_R dependence on the gas number density. All tests were conducted at ambient temperature which ranged from 287° K to 303° K with an average of 291° K. The measured T_R was compared with the corresponding ambient temperature for that particular test. The results are shown in Figure 11. An analysis of the results provided the empirical equation

$$\Delta T = \log_{10}\left(\frac{n}{n_o}\right)^{15.7} \qquad (25)$$

where ΔT is the increase in gas temperature at the point of observation due to the number density, n, dependence and n_o is the reference gas number density arbitrarily selected as $3 \times 10^{14}/cm^3$ since the results appear to converge to this value. The number density n is limited to the range, $3 \times 10^{14}/cm^3 \leqq n \leqq 3 \times 10^{16}/cm^3$.

It is assumed, based on experimental observations, that this increase in temperature is a function of number density only and is independent of gas temperature. Therefore, as the gas temperature increases the change in T_R due to number density would become relatively small.

It is also assumed that equation (25) is applicable only to the physical conditions of the tests reported here. That is, beam current, beam potential, and the distance of the observation point from the exit aperture of the electron gun. All observations were made at a point 30 cm from the gun exit aperture, beam current of 1100 μa, and beam potential, 28.5 Kv. It is important to note these conditions because of beam spreading. The greater the distance from the aperture the greater will be beam spreading for a given gas

number density. If the gas heating should be dependent on the beam electron current density, then spreading will be an important factor. It should be pointed out that changing the beam current by a factor of 2 did not change the measured T_R within experimental accuracy. Also, the temperature of the gas at the point of observation will be a function of a temperature gradient, therefore beam spreading again may be a factor since it could alter the gradient. In any case, until the exact molecular heating mechanism or process is determined, tests should be conducted for each test configuration. It is important to determine the molecular heating mechanism to determine conclusively the effects on temperature measurements in a flowing gas.

Results

Corrections in accordance with equation (25) were applied to the measured rotational temperatures. The corrected results are shown in Figure 12 which is a plot similar to Figure 10. The resultant scatter of data has been reduced from +10 percent to -4 percent, in Figure 10, to +2 percent to -6 percent, in Figure 12. Also the data are approximately grouped about a common curve. There still exists a slight difference in the data for the two different densities. This can be attributed to the inaccuracy of equation (25) due to experimental uncertainty associated with its derivation. The corrected results still indicate a slightly increasing difference between gas temperature and the measured rotational temperature. An analysis of equation (24) does not reveal any apparent sources of this difference. There are two possible causes. The first to be considered is possible experimental error. But careful analyses have been made for all the experimental apparatus and reasonable confidence has been established. The second possible source is in the formulation of the theory leading to equation (24). The excitation-transition process is complex and no direct account has been made for the effects of secondary electron excitation. Also the explicit assumption has been made that the rotational levels of the ground molecular state, $N_2X^1\Sigma_g^+$ are in thermal equilibrium. But, since a temperature difference does exist between the reference gas temperature and the measured value, then there will exist a population distribution of the rotational levels at the point of observation which is at least slightly non-Boltzmann.[9] A slight deviation from a non-Boltzmann distribution would not be detected within the obtainable experimental precision, but would affect the measured rotational temperature value.

Precision

A relative precision of ±5 percent was estimated for these measurements. The factors affecting the relative precision of the measurements were the uncertainties in gas number density, reference temperature, and the temperature values obtained from the graphic solutions. A value of ±2 percent was calculated for the effects of density and reference temperature and ±3 percent was estimated for the uncertainty of the measured temperature based on standard error values obtained from a large number of independent measurements.

CONCLUSIONS

Rotational temperature measurements performed in a static gas were found to be a function of the gas number density. An empirical equation relating the difference between the measured rotational temperature and a reference gas temperature to the gas number density was developed from experimental data. The equation was assumed to be applicable only to the physical conditions of the experiments reported here. Also, it will be necessary to determine the exact heating mechanism in order to evaluate this effect in a flowing gas environment such as a wind tunnel.

The results of this work indicated a minimum accuracy agreement with theory of +8 percent to -4 percent for rotational temperature measurements in a static gas over the 300° K to 1000° K range. Application of the corrections for the gas number density dependence of the measured temperatures resulted in a minimum accuracy agreement of 0 percent to -6 percent. Therefore, the experiments that were conducted and reported here indicate that the theory developed by Muntz for the electron beam technique for measuring gas rotational temperatures is reasonably accurate over a 300° K to 1000° K range.

NOMENCLATURE

(A)	defined by equation (18)
A_{nm}	transition probability for emission between states n and m
$A_{v'v_2''}$	transition probability for emission between vibrational energy states v' and v_2''
$A_{v'K',v_2''K_2''}$	transition probability for emission between rotational energy states K' and K_2''
B_o	rotational constant related to the vibrational level $V_1'' = 0$
$B_{v_1''}$	rotational constant related to the vibrational level v_1''
$B^2\Sigma_u^+$	represents the electronic wave function for $N_2^+B^2\Sigma_u^+$
C_e	excitation function which describes the electron-molecular excitation process

C'_e	ratio of the excitation function to depopulation rate of $N_2^+B^2\Sigma_u^+$ state
c	speed of light
$\bar{\bar{D}}(\theta,\chi,\phi)$	dyadic, function of Euler angles
$E_{K_1''}$	characteristic energy of K_1'' rotational energy level
$E_{v_1''}$	characteristic energy of v_1'' vibrational energy level
e	electron charge
$e_{P'}, e_{P''}$	primary electron
e_S	secondary electron
$F(K_1'')$	rotational term[7]
$[G]$	defined by equation (23)
$G_o(V_1'')$	vibrational term[7]
h	Planck's constant
I_{em}^{nm}	intensity of emission for transitions between n and m states
$I_{K'K_2''}$	intensity of emission for transitions between K' and K" rotational energy levels
I_o	reference intensity of emission
$I_{v'v_2''}$	intensity of emission for transitions between v' and v_2'' vibrational energy levels
J',J"	quantum number of the total angular momentum
K'	quantum number of rotational energy level of $N_2^+B^2\Sigma_u^+$
K_1''	quantum number of rotational energy level of $N_2X^1\Sigma_g^+$
K_2''	quantum number of rotational energy level of $N_2^+X^2\Sigma_g^+$
k	Boltzmann's constant
M',M"	quantum number of a component of total angular momentum
N_n	number density population of state n
N_o	steady-state number density population of $N_2X^1\Sigma_g^+$
$N_{K'}$	steady-state number density population of a rotational energy level K' of $N_2^+B^2\Sigma_u^+$
$N_{K_1''}$	steady-state number density population of a rotational energy level K" of $N_2X^1\Sigma_g^+$
$N_{v'}$	steady-state number density population of a vibrational energy level v' of $N_2^+B^2\Sigma_u^+$
$N_{v_1''}$	steady-state number density population of a vibrational energy level v_1'' of $N_2^+B^2\Sigma_u^+$
N_2	neutral nitrogen
N_2^+	ionized nitrogen
n	gas number density
n_o	reference gas number density
$N_2^+B^2\Sigma_u^+$	excited ion state of N_2^+
$N_2X^1\Sigma_g^+$	ground state of N_2
$N_2^+X^2\Sigma_g^+$	ground state of N_2^+
P_R^a	relative rotational line strength for excitation
P_{RR}^a, P_{RP}^a	relative rotational line strength for excitation, R branch and P branch, respectively
P_R^e	relative rotational line strength for emission
P_{RR}^e, P_{RP}^e	relative rotational line strength for emission, R branch and P branch, respectively
$P_{v'v''}$	band strength
Q_r	rotational partition function
Q_v	vibrational partition function
q	momentum transfer term
$q_{v'v''}$	Franck-Condon factor
R_{ij}^e	electronic transition moment for electronic states i and j
$\bar{r}_i$	position vector of ith orbital electron

r_n	nuclei separation
$\bar{r}_1$	position vector of primary electron with respect to point of observation
r_{12}	distance between primary and secondary electrons
r_{1i}	distance between primary and ith orbital electrons
$\bar{r}_2$	position vector of secondary electron with respect to point of observation
$\bar{r}_2'$	position vector of secondary electron with respect to molecular axis
$S_{K''}^{K'}$	Hönl-London factor
T_R	rotational temperature
T_v	vibrational temperature
v'	vibrational energy state of $N_2^+B^2\Sigma_u^+$
v_o', v_1'	vibrational energy states of $N_2^+B^2\Sigma_u^+$
v_1''	vibrational energy state of $N_2X^1\Sigma_g^+$
v_2''	vibrational energy state of $N_2^+X^2\Sigma_g^+$
X	a constant of $A_{v'K',v_2''K_2''}$
$X^1\Sigma_g^+$	represents the electronic wavefunction for $N_2X^1\Sigma_g^+$
Z,Z',Z"	constants defined in the text
θ,χ,φ	Euler angles
Λ',Λ''	quantum number of the resultant electronic orbital angular momentum
ν_{nm}	wave number of nm transition
$\sigma_u 2s$	angular characteristics of an orbital electron of $N_2X^1\Sigma_g^+$
Ψ_e	electronic state wave function
Ψ_{evJAM}	molecular wave function
Ψ_{JAM}	rotational state wave function
Ψ_v	vibrational state wave function

ACKNOWLEDGMENT

The author would like to express his appreciation to Stewart L. Ocheltree and Dr. George S. Ofelt for their helpful assistance in the evaluation of the work reported here and in the preparation of this paper.

REFERENCES

1. Muntz, E. P., "Static Temperature Measurements in a Flowing Gas," The Physics of Fluids, 5, 80-90, 1962.

2. Sebacher, D. I.; and Duckett, R. J., "A Spectrographic Analysis of a One-Foot Hypersonic-Arc-Tunnel Airstream Using an Electron Beam Probe," NASA TR R-214, 1964.

3. Petrie, S. L.; Pierce, G. A.; and Fishburne, E. S., "Analysis of the Thermochemical State of an Expanded Air Plasma," The Ohio State University Research Foundation, Technical Report AFFDL-TR-64-191, 1965.

4. Robben, F.; and Talbot, L., "Measurements of Rotational Temperatures in a Low Density Wind Tunnel," The Physics of Fluids, 9, 644-652, 1966.

5. Muntz, E. P.; and Abel, S. J., "The Direct Measurement of Static Temperatures in Stock Tunnel Flows," Third Hypersonic Technique Symposium, 1964.

6. Herzberg, G., Spectra of Diatomic Molecules, D. Van Nostrand and Co., Princeton, N.J., 1950.

7. Landau, L. D.; and Lifshitz, E. M., Quantum Mechanics: Non-Relativistic Theory, Addison-Wesley, Reading, Mass., 1958.

8. Fraser, P. A., "A Method of Determining the Electronic Transition Moment for Diatomic Molecules," Can. J. Phys., 32, 515-521, 1954.

9. Kennard, E. H., Kinetic Theory of Gases, McGraw-Hill Book Co., Inc., New York, 1938.

TABLE 1.- $\log_{10}\left\{[G]\left(\upsilon/\upsilon_0\right)^4\right\}$ VALUES FOR O-O BAND

O-O BAND

T(R)	50.0	75.0	100.0	125.0	150.0	175.0	200.0	225.0	250.0	275.0	300.0	325.0	350.0	400.0
K'														
0.	-0.0507	-0.0341	-0.0258	-0.0208	-0.0175	-0.0151	-0.0133	-0.0120	-0.0109	-0.0099	-0.0092	-0.0086	-0.0080	-0.0071
1.0	-0.0445	-0.0312	-0.0241	-0.0196	-0.0166	-0.0144	-0.0127	-0.0114	-0.0103	-0.0095	-0.0088	-0.0081	-0.0076	-0.0068
2.0	-0.0325	-0.0257	-0.0208	-0.0174	-0.0150	-0.0131	-0.0117	-0.0105	-0.0096	-0.0088	-0.0081	-0.0076	-0.0071	-0.0063
3.0	-0.0152	-0.0178	-0.0162	-0.0144	-0.0127	-0.0114	-0.0103	-0.0094	-0.0086	-0.0079	-0.0073	-0.0068	-0.0064	-0.0057
4.0	0.0073	-0.0073	-0.0102	-0.0104	-0.0099	-0.0092	-0.0085	-0.0079	-0.0073	-0.0068	-0.0064	-0.0060	-0.0056	-0.0050
5.0	0.0343	0.0054	-0.0027	-0.0054	-0.0063	-0.0065	-0.0064	-0.0061	-0.0058	-0.0055	-0.0052	-0.0049	-0.0046	-0.0042
6.0	0.0653	0.0203	0.0060	0.0004	-0.0022	-0.0033	-0.0038	-0.0040	-0.0040	-0.0040	-0.0039	-0.0037	-0.0036	-0.0032
7.0	0.0998	0.0373	0.0161	0.0070	0.0026	0.0003	-0.0010	-0.0017	-0.0021	-0.0023	-0.0024	-0.0024	-0.0023	-0.0022
8.0	0.1372	0.0562	0.0274	0.0145	0.0080	0.0044	0.0023	0.0010	0.0002	-0.0003	-0.0007	-0.0009	-0.0010	-0.0011
9.0	0.1772	0.0769	0.0398	0.0229	0.0140	0.0090	0.0059	0.0040	0.0027	0.0018	0.0012	0.0008	0.0005	0.0002
10.0	0.2192	0.0991	0.0533	0.0320	0.0206	0.0140	0.0099	0.0072	0.0054	0.0041	0.0032	0.0026	0.0021	0.0015
11.0	0.2630	0.1228	0.0679	0.0418	0.0278	0.0194	0.0142	0.0107	0.0084	0.0067	0.0055	0.0046	0.0039	0.0030
12.0	0.3081	0.1477	0.0835	0.0524	0.0354	0.0253	0.0188	0.0145	0.0115	0.0094	0.0078	0.0067	0.0058	0.0045
13.0	0.3544	0.1739	0.1000	0.0638	0.0437	0.0316	0.0239	0.0186	0.0150	0.0124	0.0104	0.0089	0.0078	0.0062
14.0	0.4016	0.2010	0.1173	0.0757	0.0524	0.0383	0.0292	0.0230	0.0186	0.0155	0.0131	0.0113	0.0100	0.0080
15.0	0.4496	0.2291	0.1355	0.0883	0.0617	0.0454	0.0348	0.0276	0.0225	0.0188	0.0160	0.0139	0.0122	0.0099
16.0	0.4981	0.2580	0.1543	0.1015	0.0714	0.0529	0.0408	0.0325	0.0266	0.0223	0.0191	0.0166	0.0147	0.0119
17.0	0.5471	0.2876	0.1738	0.1152	0.0816	0.0607	0.0471	0.0377	0.0309	0.0260	0.0223	0.0194	0.0172	0.0140
18.0	0.5965	0.3177	0.1940	0.1295	0.0922	0.0690	0.0536	0.0431	0.0355	0.0299	0.0257	0.0224	0.0199	0.0162
19.0	0.6462	0.3485	0.2147	0.1443	0.1032	0.0775	0.0605	0.0487	0.0402	0.0340	0.0292	0.0256	0.0227	0.0185
20.0	0.6961	0.3797	0.2359	0.1595	0.1147	0.0864	0.0677	0.0546	0.0452	0.0382	0.0329	0.0288	0.0256	0.0209
21.0	0.7462	0.4113	0.2576	0.1752	0.1265	0.0957	0.0751	0.0607	0.0504	0.0427	0.0368	0.0323	0.0287	0.0234
22.0	0.7964	0.4433	0.2797	0.1913	0.1387	0.1052	0.0828	0.0671	0.0557	0.0473	0.0408	0.0358	0.0318	0.0260
23.0	0.8468	0.4756	0.3022	0.2077	0.1512	0.1151	0.0908	0.0737	0.0613	0.0521	0.0450	0.0395	0.0351	0.0287

T(R)	450.0	500.0	550.0	600.0	650.0	700.0	750.0	800.0	850.0	900.0	950.0	1000.0	1050.0	1100.0
K'														
0.	-0.0064	-0.0059	-0.0054	-0.0050	-0.0047	-0.0045	-0.0042	-0.0040	-0.0038	-0.0037	-0.0035	-0.0034	-0.0033	-0.0032
1.0	-0.0061	-0.0055	-0.0051	-0.0047	-0.0044	-0.0042	-0.0039	-0.0037	-0.0035	-0.0034	-0.0032	-0.0031	-0.0030	-0.0029
2.0	-0.0056	-0.0051	-0.0047	-0.0043	-0.0040	-0.0038	-0.0036	-0.0034	-0.0032	-0.0030	-0.0029	-0.0028	-0.0026	-0.0025
3.0	-0.0051	-0.0046	-0.0042	-0.0039	-0.0036	-0.0034	-0.0032	-0.0030	-0.0028	-0.0027	-0.0025	-0.0024	-0.0023	-0.0022
4.0	-0.0045	-0.0041	-0.0037	-0.0034	-0.0031	-0.0029	-0.0027	-0.0025	-0.0024	-0.0022	-0.0021	-0.0020	-0.0019	-0.0018
5.0	-0.0038	-0.0034	-0.0031	-0.0028	-0.0026	-0.0024	-0.0022	-0.0021	-0.0019	-0.0018	-0.0017	-0.0016	-0.0015	-0.0014
6.0	-0.0030	-0.0027	-0.0024	-0.0022	-0.0020	-0.0018	-0.0017	-0.0015	-0.0014	-0.0013	-0.0012	-0.0011	-0.0010	-0.0009
7.0	-0.0021	-0.0019	-0.0017	-0.0015	-0.0014	-0.0012	-0.0011	-0.0010	-0.0009	-0.0008	-0.0007	-0.0006	-0.0005	-0.0004
8.0	-0.0011	-0.0010	-0.0009	-0.0008	-0.0007	-0.0006	-0.0005	-0.0004	-0.0003	-0.0002	-0.0001	-0.0000	0.0000	0.0001
9.0	0.0000	-0.0000	-0.0000	-0.0000	0.0001	0.0001	0.0002	0.0003	0.0003	0.0004	0.0005	0.0005	0.0006	0.0006
10.0	0.0012	0.0010	0.0009	0.0009	0.0009	0.0009	0.0009	0.0009	0.0010	0.0010	0.0011	0.0011	0.0012	0.0012
11.0	0.0024	0.0021	0.0019	0.0018	0.0017	0.0017	0.0017	0.0017	0.0017	0.0017	0.0017	0.0018	0.0018	0.0018
12.0	0.0038	0.0033	0.0030	0.0028	0.0026	0.0025	0.0025	0.0024	0.0024	0.0024	0.0024	0.0024	0.0025	0.0025
13.0	0.0052	0.0046	0.0041	0.0038	0.0036	0.0034	0.0033	0.0033	0.0032	0.0032	0.0032	0.0032	0.0032	0.0032
14.0	0.0067	0.0059	0.0053	0.0049	0.0046	0.0044	0.0042	0.0041	0.0040	0.0040	0.0039	0.0039	0.0039	0.0039
15.0	0.0084	0.0073	0.0066	0.0061	0.0057	0.0054	0.0052	0.0050	0.0049	0.0048	0.0047	0.0047	0.0046	0.0046
16.0	0.0101	0.0088	0.0079	0.0073	0.0068	0.0065	0.0062	0.0060	0.0058	0.0057	0.0056	0.0055	0.0054	0.0054
17.0	0.0119	0.0104	0.0093	0.0086	0.0080	0.0076	0.0072	0.0070	0.0067	0.0066	0.0065	0.0064	0.0063	0.0062
18.0	0.0137	0.0120	0.0108	0.0099	0.0092	0.0087	0.0083	0.0080	0.0077	0.0075	0.0074	0.0072	0.0071	0.0070
19.0	0.0157	0.0137	0.0123	0.0113	0.0105	0.0099	0.0094	0.0091	0.0088	0.0085	0.0083	0.0082	0.0080	0.0079
20.0	0.0177	0.0155	0.0139	0.0127	0.0118	0.0111	0.0106	0.0102	0.0098	0.0095	0.0093	0.0091	0.0089	0.0088
21.0	0.0199	0.0174	0.0156	0.0142	0.0132	0.0124	0.0118	0.0113	0.0109	0.0106	0.0103	0.0101	0.0099	0.0097
22.0	0.0221	0.0193	0.0173	0.0158	0.0147	0.0138	0.0131	0.0125	0.0120	0.0117	0.0114	0.0111	0.0109	0.0107
23.0	0.0244	0.0213	0.0191	0.0174	0.0162	0.0152	0.0144	0.0137	0.0132	0.0128	0.0125	0.0122	0.0119	0.0117

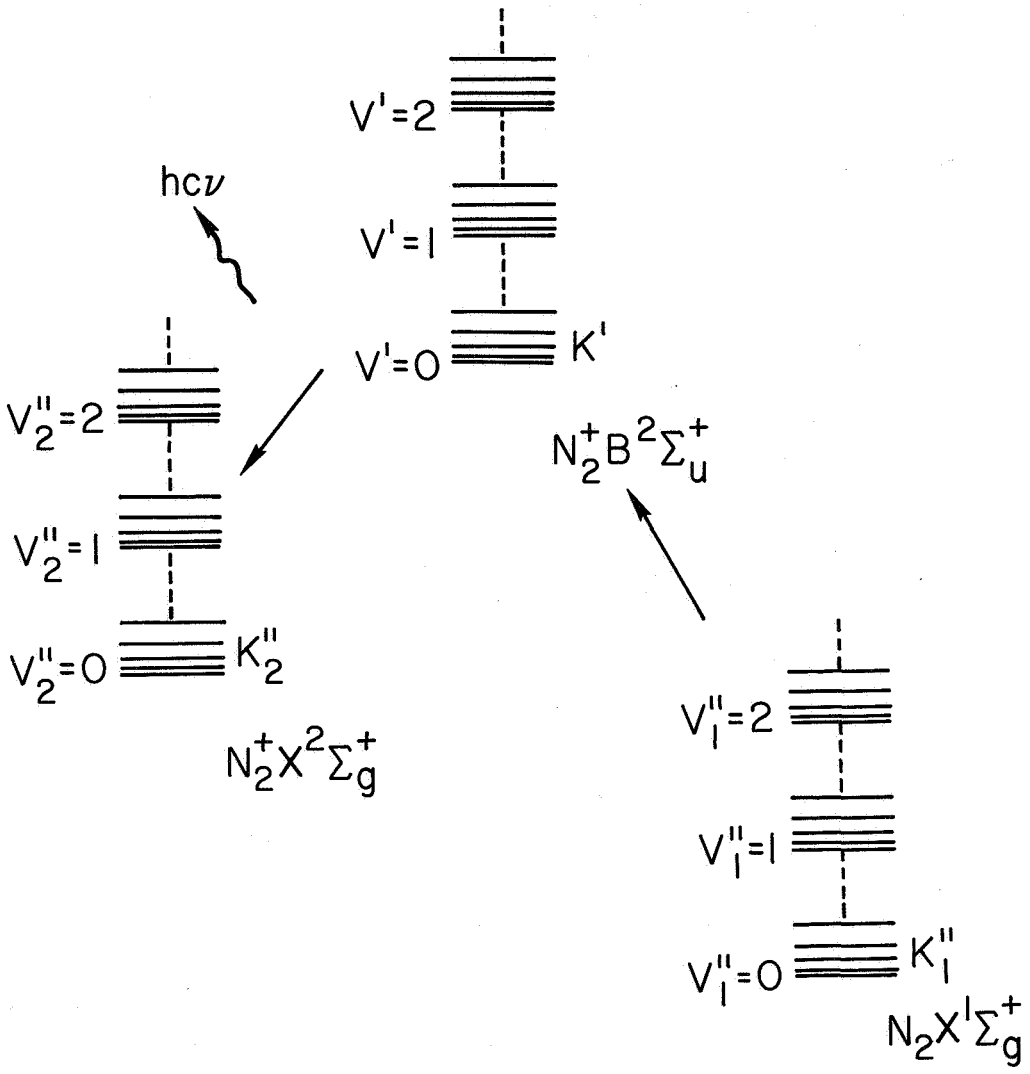

Figure 1.- Partial energy level diagram of nitrogen.

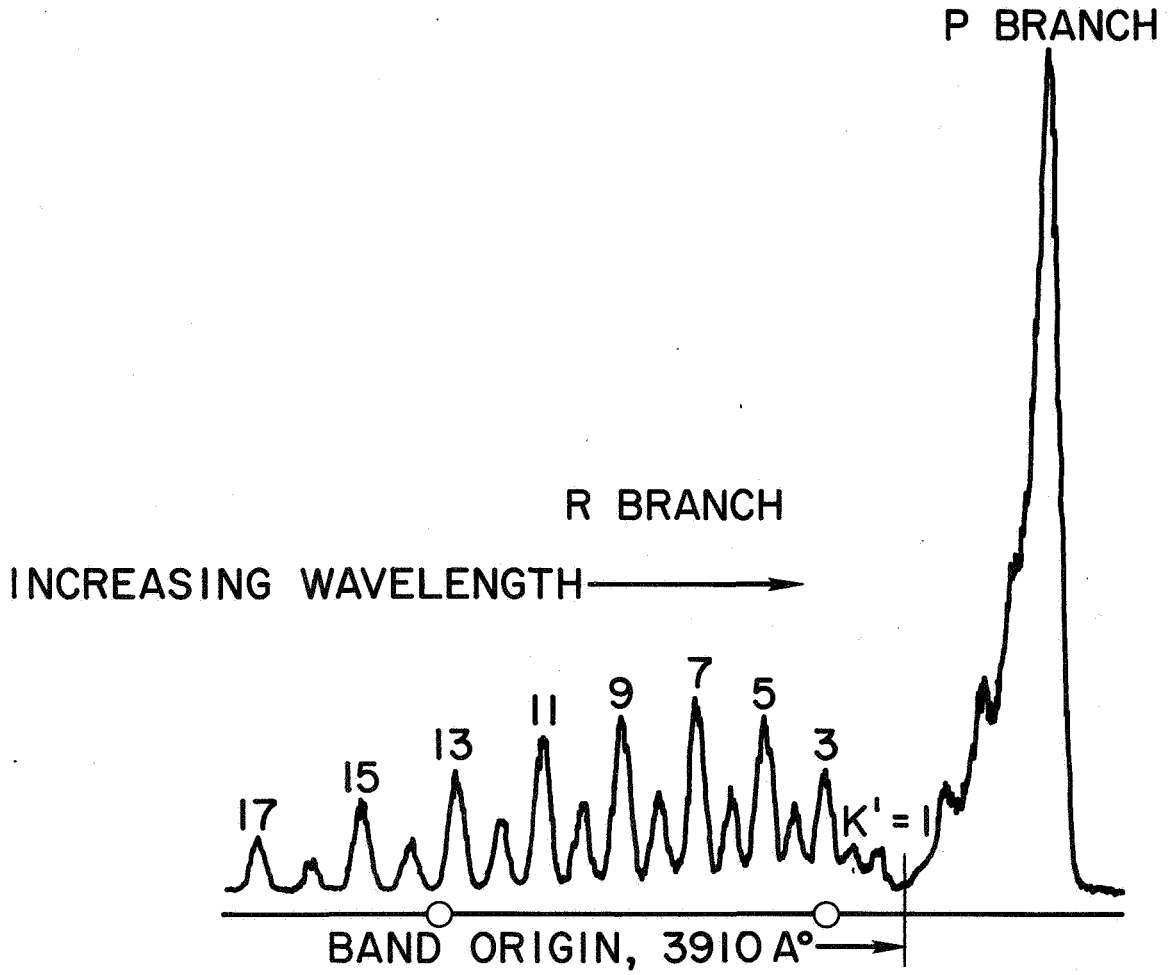

Figure 2.- Spectrometer trace N_2^+ 0-0 band rotational structure, ≈300° K.

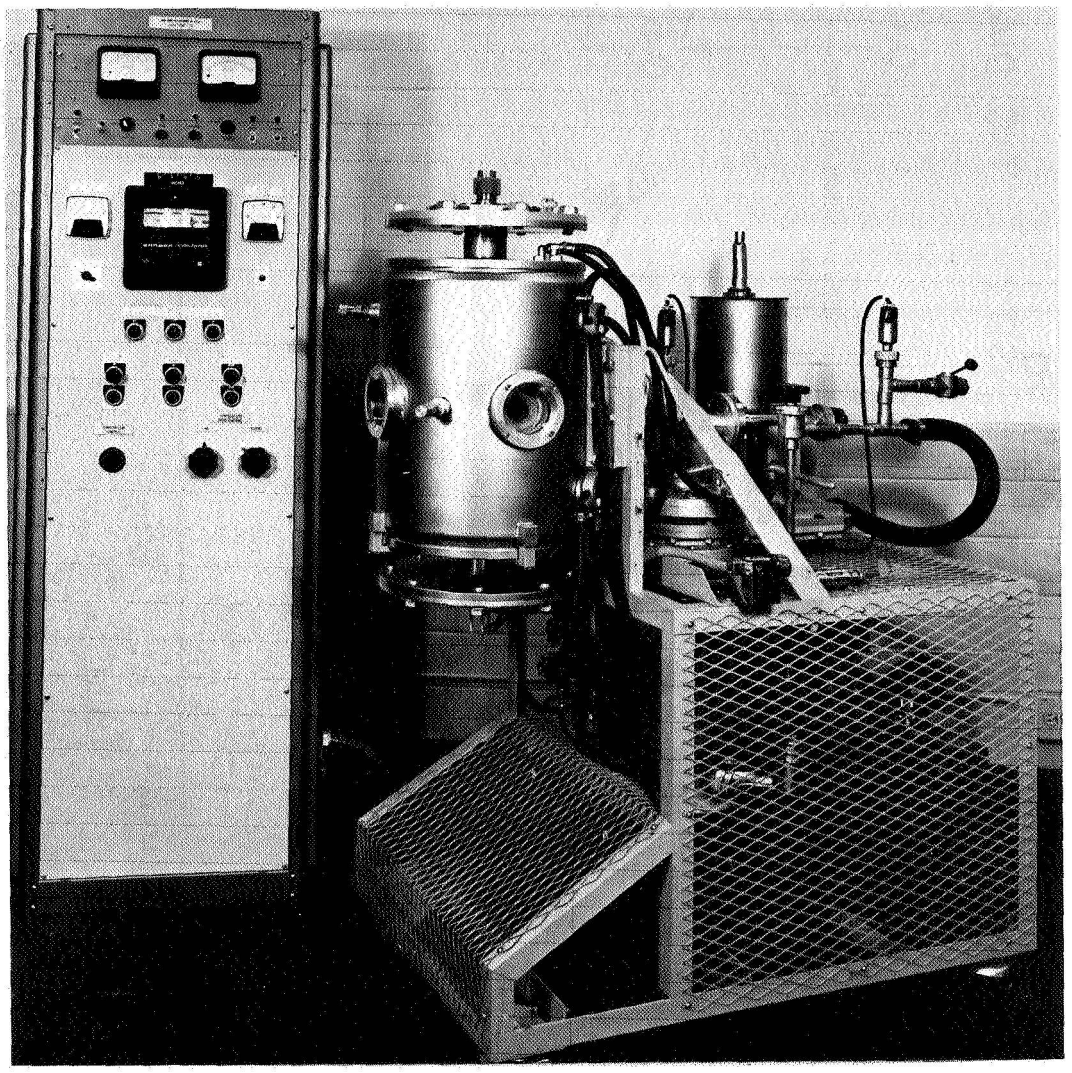

Figure 3.- Test gas temperature and pressure control system.

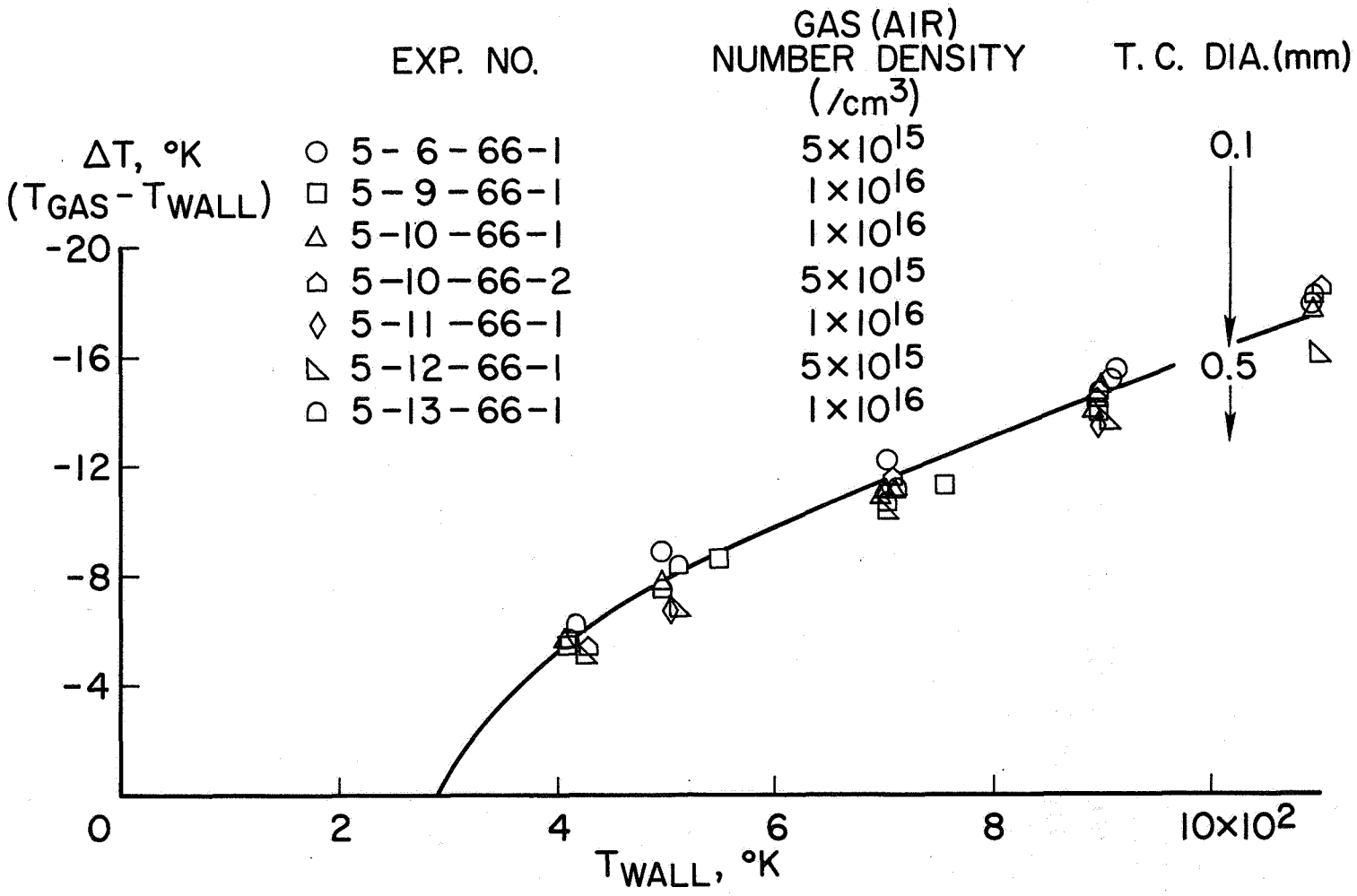

Figure 4.- Test chamber wall temperature versus difference between wall temperature and gas temperature.

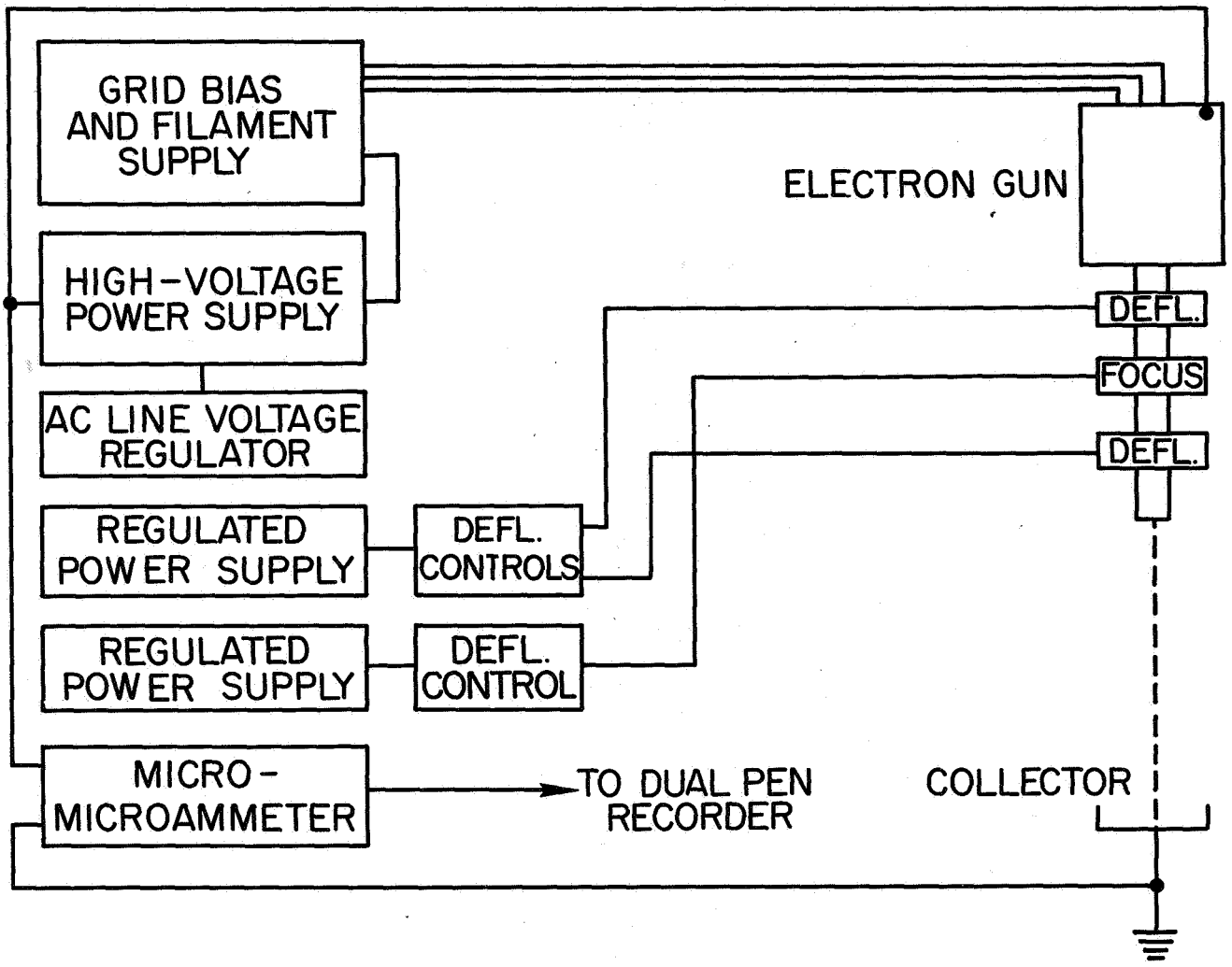

Figure 5.- Block diagram, electron beam system.

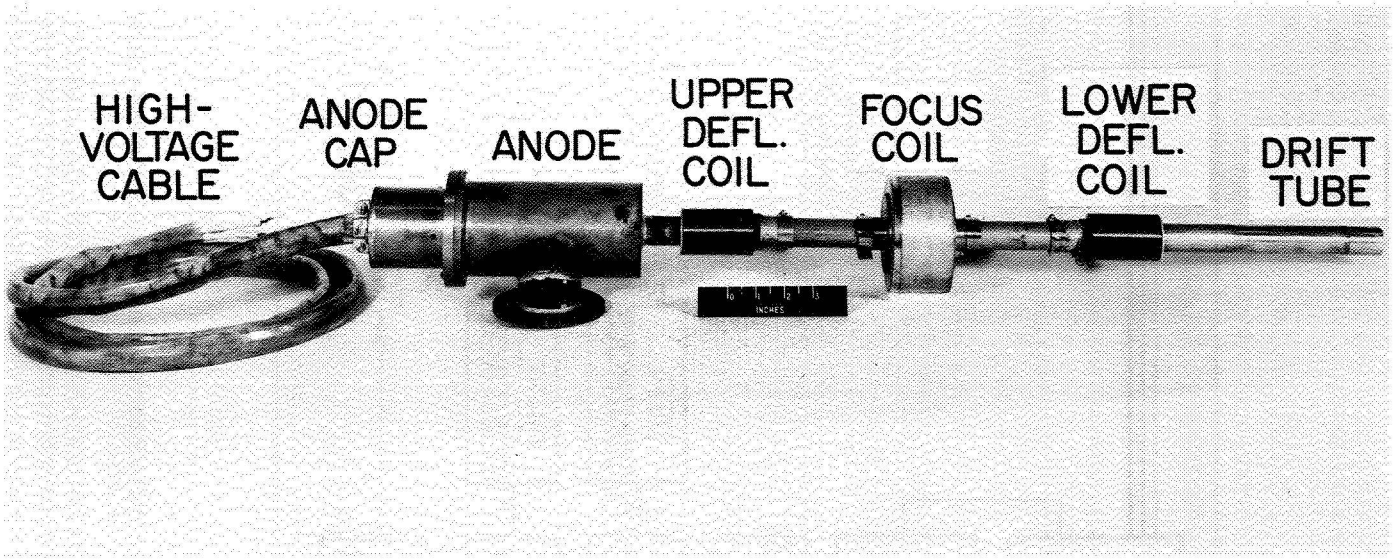

Figure 6.- Electron gun and anode assembly.

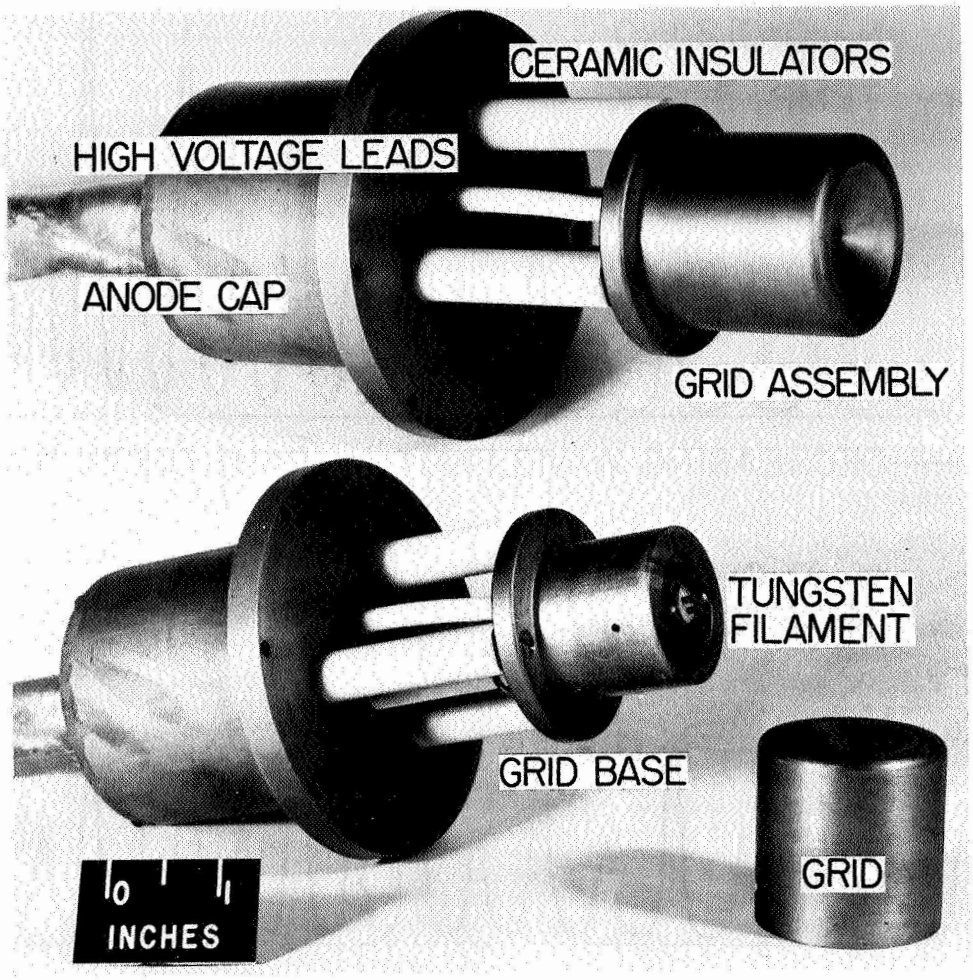

Figure 7.- Electron gun.

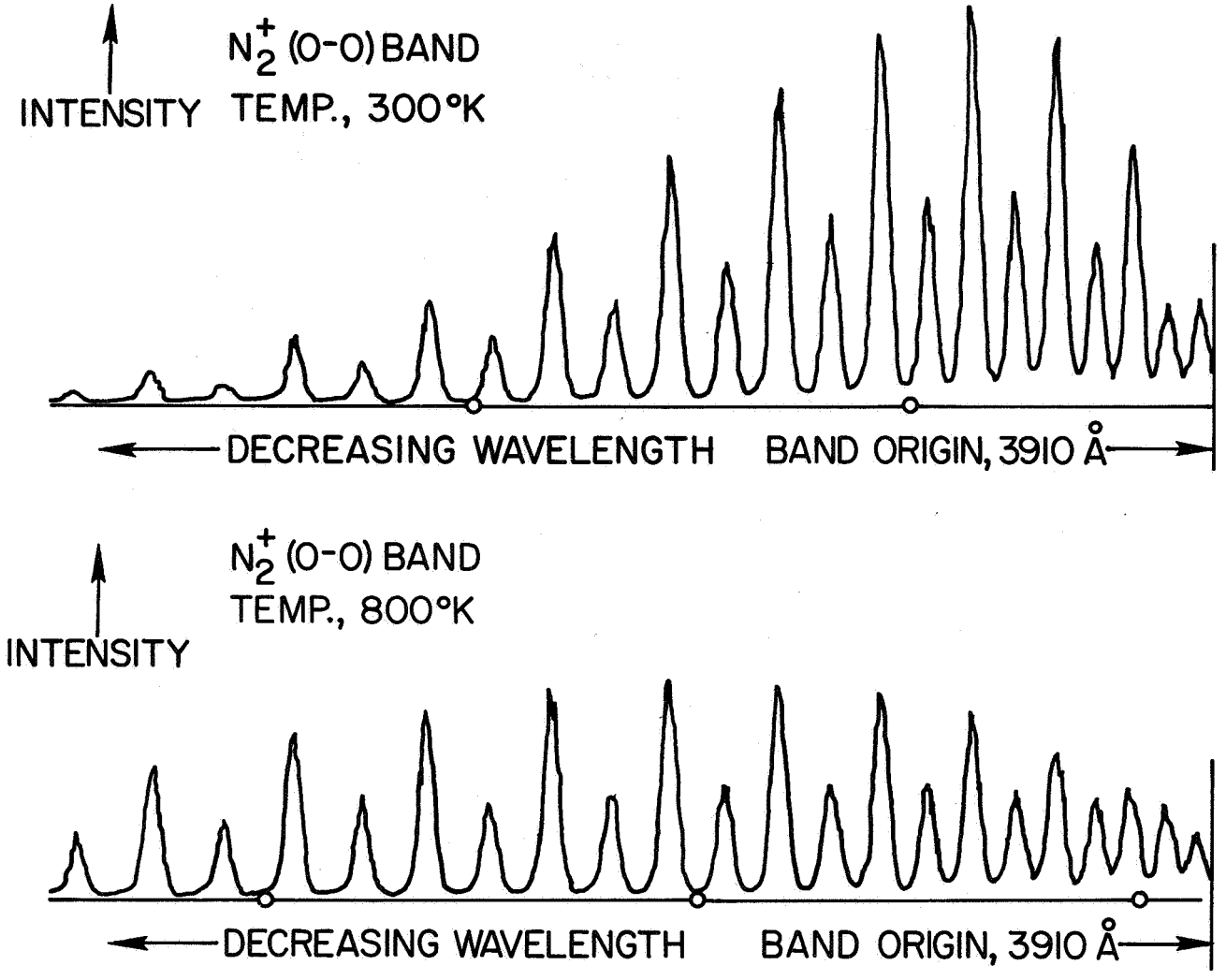

Figure 8.- Typical spectrum, N_2^+(0-0) band R-branch.

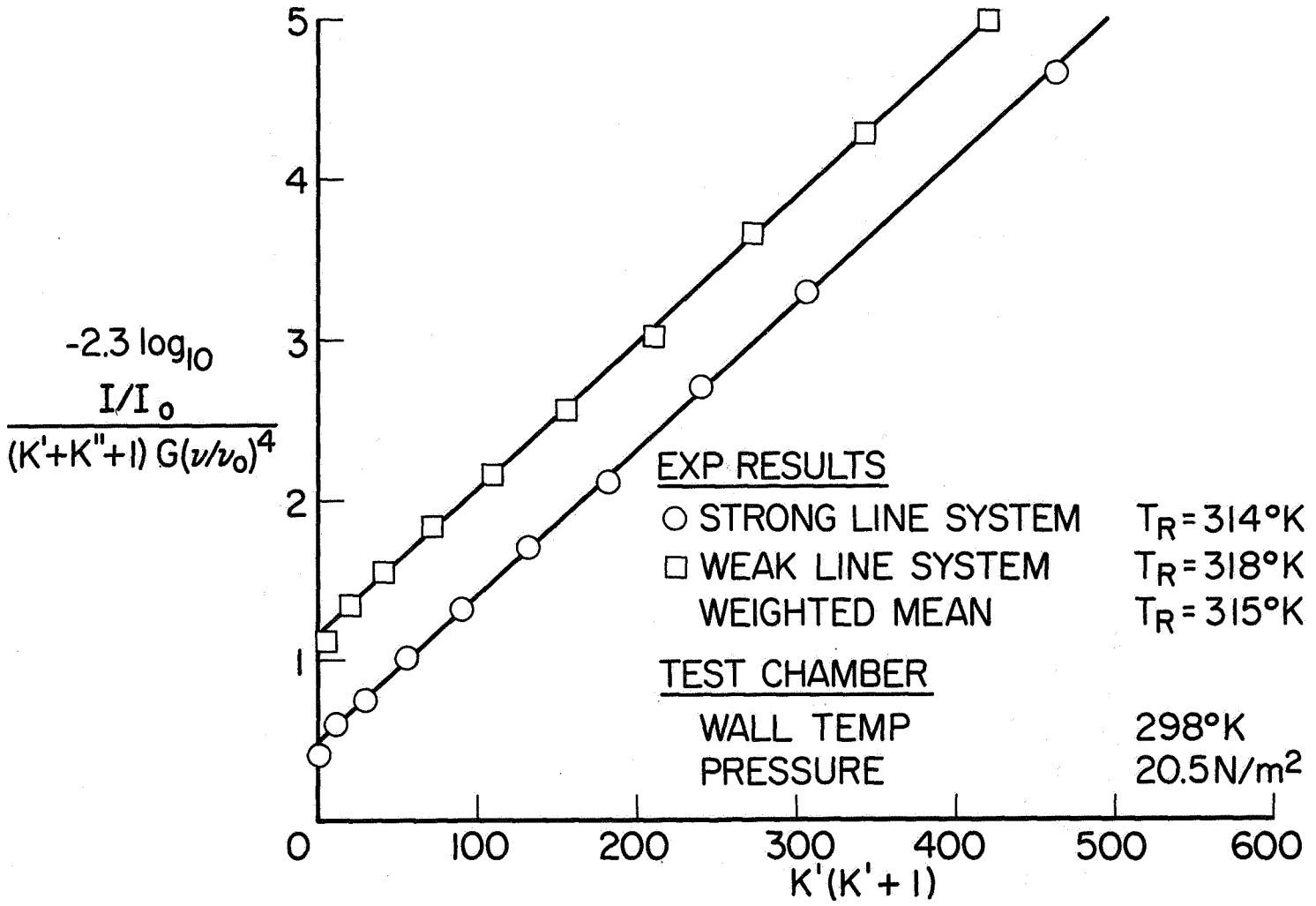

Figure 9.- N_2^+ 0-0 band data for 300° K experiment for T_R measurements.

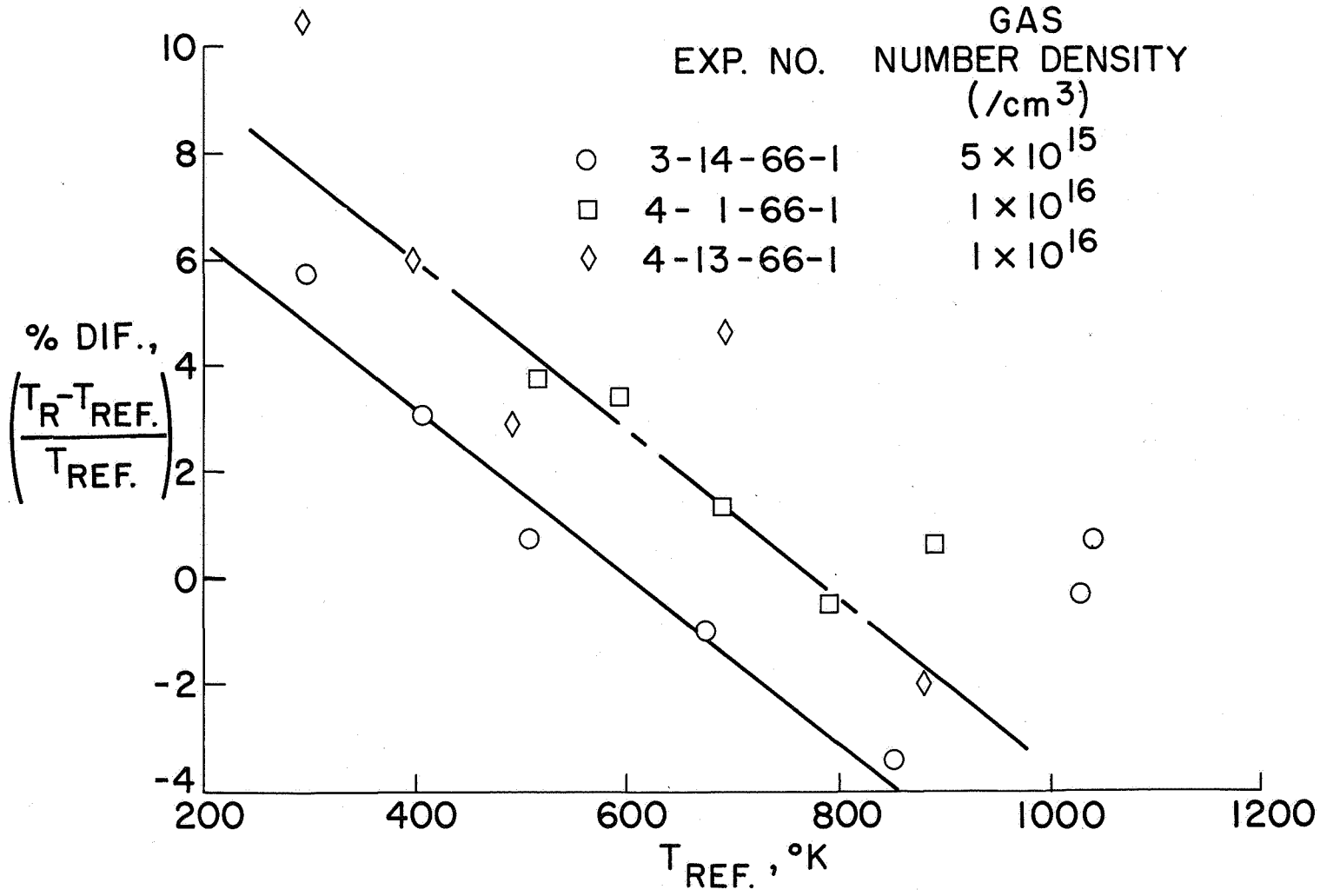

Figure 10.- Results of 300° K to 1000° K T_R tests.

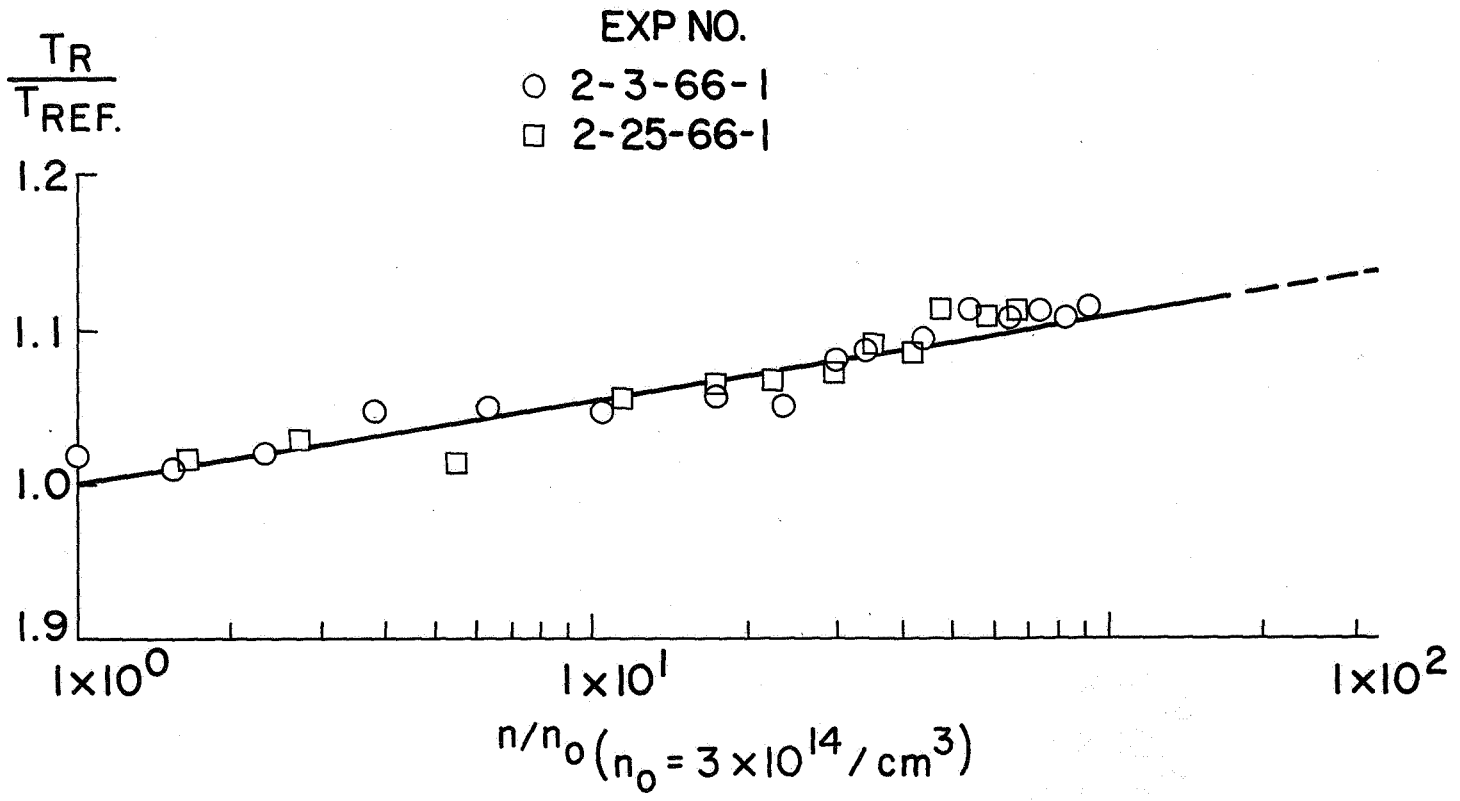

Figure 11.- T_R gas number density dependence.

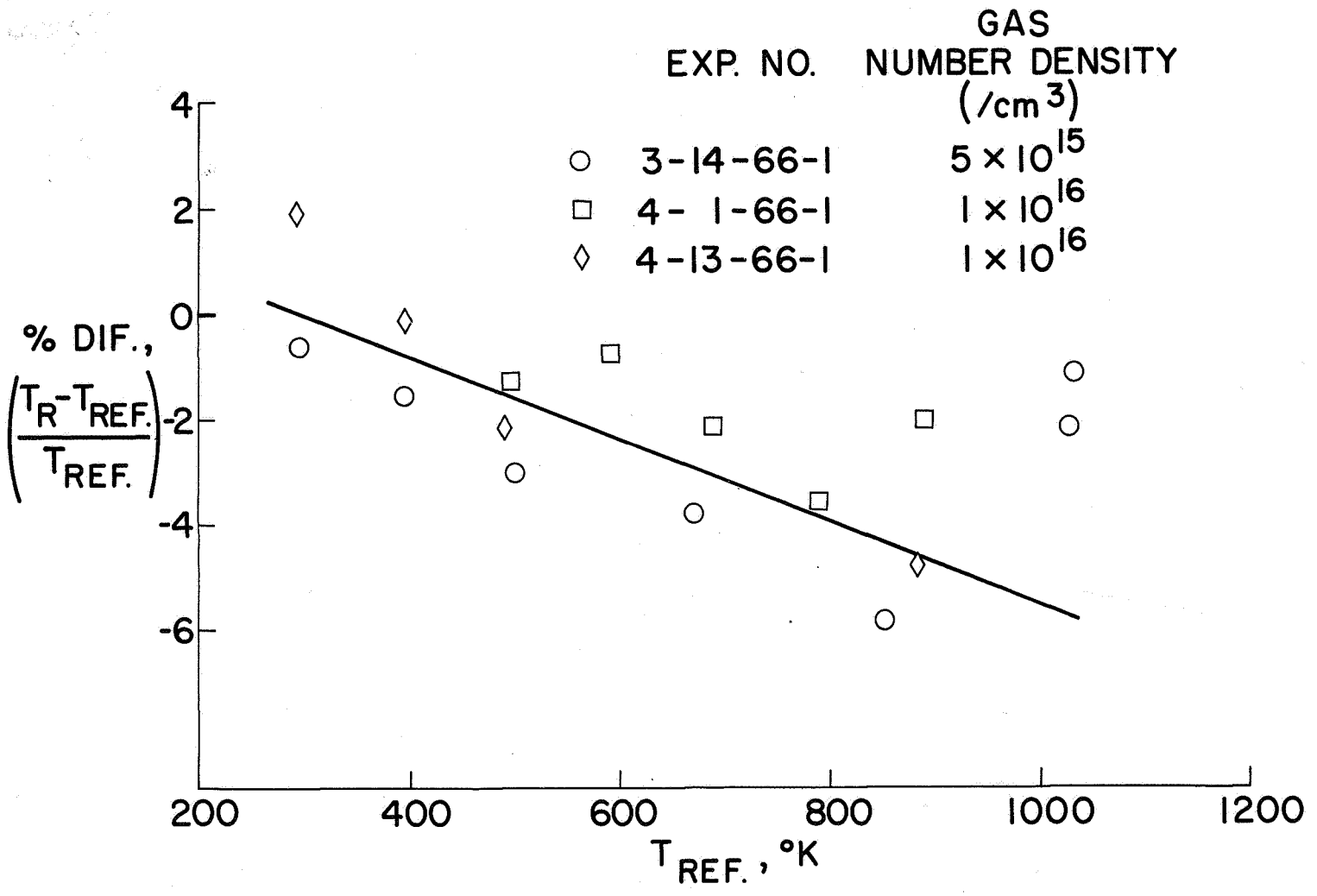

Figure 12.- Results of 300° K to 1000° K T_R tests corrected for gas number density effect.